Communication

Activation of Carbon Nitride Solids by Protonation: Morphology Changes, Enhanced Ionic Conductivity, and Photoconduction Experiments

Yuanjian Zhang, Arne Thomas, Markus Antonietti, and Xinchen Wang

J. Am. Chem. Soc., **2009**, 131 (1), 50-51• DOI: 10.1021/ja808329f • Publication Date (Web): 10 December 2008

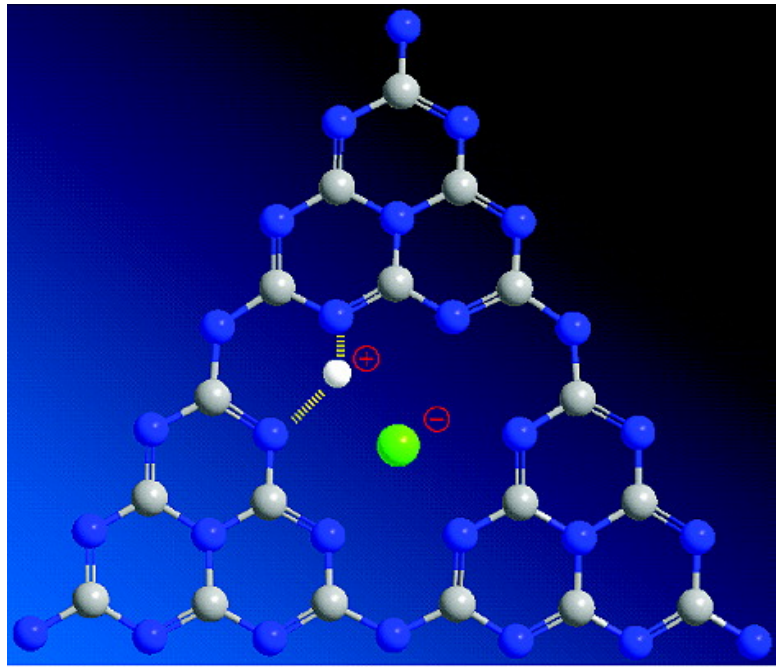

J|A|C|S COMMUNICATIONS

Published on Web 12/10/2008

Activation of Carbon Nitride Solids by Protonation: Morphology Changes, Enhanced Ionic Conductivity, and Photoconduction Experiments

Yuanjian Zhang,* Arne Thomas, Markus Antonietti, and Xinchen Wang

Max Planck Institute of Colloids and Interfaces, Research Campus Golm, D-14424 Potsdam, Germany

Received October 28, 2008; E-mail: Yuanjian.Zhang@mpikg.mpg.de

Greater efforts have recently been devoted to covalently bonded carbon nitride materials,[1−3] which have numerous potential applications ranging from semiconductors to fuel cells. For example, bulk graphitic-C_3N_4 (g-C_3N_4), the most stable allotrope at ambient conditions, has been approached by condensation from suitable molecular precursors,[4] and the species made along this condensation route were found to be active for metal-free carbon dioxide-activation,[5] as a reactant for metal nitride nanoparticle synthesis,[6] and even as a catalyst for the direct photochemical splitting of water.[7] However, all carbon nitrides, even the polymeric C_3N_4 melon,[1] are insoluble, which makes characterization and processing difficult.

It is widely accepted to date that tri-*s*-triazine is the primary building block of carbon nitrides, polymers, and networks. Finer details of local structure and composition of as synthesized materials are however lacking in many cases, which results also in limitations and uncertainties in potential applications. Also, the chemistry of the as-synthesized carbon nitride was hardly touched, and some of the handicaps of g-C_3N_4 might be circumvented by postfunctionalization, as for instance exemplified by carbon nanotubes or fullerenes where functionalization has made those materials applicable. Indeed, postfunctionalization would allow introduction of functional groups into g-C_3N_4 after the lattice is formed at elevated temperatures. Among others, direct protonation of base functionalities is a convenient modification route. This follows nitrogen-rich engineering plastics which can be prepared and processed in concentrated mineral acids,[8] and direct protonation had also been used to disperse and process CNTs.[9] For polymer semiconductors, such as polyaniline, protonation is used to tune the electronic structure,[10] and polyamidoamine dendrimers were protonated to enhance proton conductivity and photoluminescence properties.[11] Herein, we report that carbon nitrides could be reversibly protonated by strong mineral acids, thus modifying solubility/dispersability, electronic structure, and surface area. The potential of this strategy is further illustrated by preparation of a new series of g-C_3N_4 based functional hybrid materials via counteranion exchange.

In a first set of experiments, it was tested that protonation with strong acids does not chemically disintegrate carbon nitrides. The polymeric C_3N_4 was prepared as described in ref 3. Milling the product and stirring it with HCl (37%) for 3 h at room temperature gave an opaque dispersion. The infrared (FT-IR) spectrum of protonated g-C_3N_4 (with 37% HCl, g-C_3N_4−H^+Cl^-) shows typical C−N heterocycle stretches in the ∼1100−1600 cm^{-1} region which are related to the extended network connection; no peaks corresponding to an −amide or −OH group which could be related to broken fragments were found (Figure S1). Moreover, the XRD pattern of the g-C_3N_4−H^+Cl^- still contains the characteristic (002) interlayer-stacking peak; e.g., the graphite-like structure of g-C_3N_4 was retained after the protonation (Figure 1a).

Direct evidence of the protonation came from the increased hydrogen content of protonated g-C_3N_4, as determined by elemental analysis. Considering that g-C_3N_4 is composed of a large number of nitrogen with potential base functionality (−C−N−), controllable and reversible protonation is only a question of acid strength. The Figure 1a inset shows that the quantity of hydrogen could be well tuned by varying HCl concentration. This is the typical behavior of a weak base. On the other hand, HCl in the g-C_3N_4−H^+Cl^- could also be eliminated continuously by heating at different temperatures. The zeta-potential of g-C_3N_4 dispersions in water was shifted after contact with HCl from negative to positive surface charges from −47.4 to +30 mV, again proving successful protonation. Interestingly, the protonation turned yellow g-C_3N_4 into practically white g-C_3N_4−H^+Cl^- and *vice versa* (Figure S2). UV−vis spectra (Figure 1b) indicate that the optical band gap and thereby the semiconductor properties are maintained but gradually blue-shifted from 481 to 424 nm following different degrees of protonation. This is in agreement with photoluminescence spectra in which the emission peak is blue-shifted from 465 to 432 nm after the protonation (Figure 1b inset).

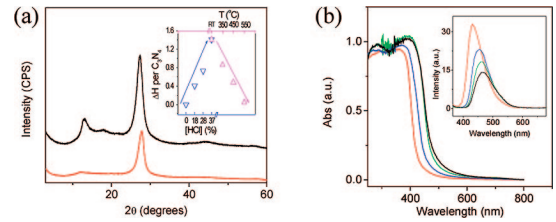

Figure 1. (a) XRD patterns g-C_3N_4 of before (black) and after (red) the protonation with 37% HCl. Inset: Increased H number per C_3N_4 unit when g-C_3N_4 reacted with 18%, 28%, and 37% HCl and recovered by heating at 350, 450, and 550 °C in N_2, respectively. (b) UV−vis spectra and photoluminescence spectra (inset) of g-C_3N_4 before (black) and after reaction with 18% (green), 28% (blue), and 37% HCl (red), respectively.

Adding protons also led to better dispersion in aqueous solutions and, depending on the degree of protonation of the primary tri-s-triazine units, even partial delamination and grain disintegration. The BET surface area of g-C_3N_4−H^+Cl^- increased in a model case from 8 to 30 m^2/g, while the higher surface area can be kept through the aforementioned dehydrohalogenation occurring at 550 °C. SEM images indicate the typical slate-like, stacked lamellar texture of milled g-C_3N_4 (Figure 2a), where the lamellar character is indicated

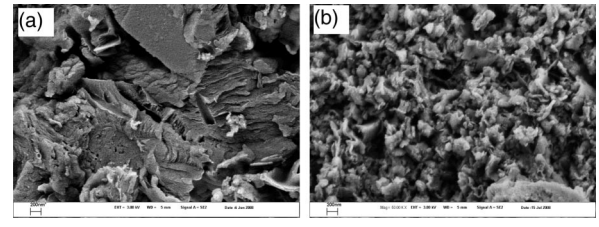

Figure 2. SEM images of as-prepared (a) and regenerated (b) g-C_3N_4 (b). Scale bars are 200 nm.

10.1021/ja808329f CCC: $40.75

by its preferential cleavage planes. The picture of the regenerated g-C_3N_4 (Figure 2b) indicates a breaking up of both sheets and stacks as well as the development of an open texture between the single sheet-like nanocrystals. Due to its partly imperfect polymer-like structure, the as-obtained C_3N_4 might be broken up from its defects by protonation while the characteristic interplanar stacking structure remains; i.e., delamination is far from being complete. Thus, the protonation provided an economic post-treatment to modify the surface area and the morphology of g-C_3N_4, which is relevant for most potential solid state applications, e.g., in solar cells and photocatalytic water splitting.

The recent observation that g-C_3N_4 can serve as an effective, all organic water splitting photocatalyst[7] was performed with the milled powder. It is found that the H_2 production efficacy of the proton-activated g-C_3N_4 in visible light increased by a factor of 2 (data not presented). Sintering of the protonated powders throughout dehydrohalogenation also enabled the layout of photoelectrically better performing films. Thus, it was possible to measure the photoconductivity of a g-C_3N_4 directly on films made of sintered protonated powders (Figure 3a).

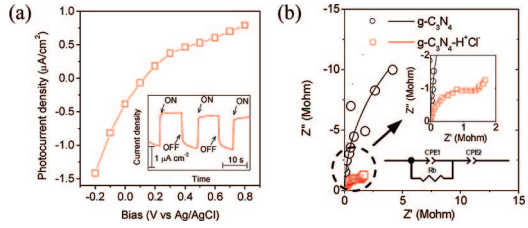

Figure 3. (a) Photocurrent-applied potential dependence at regenerated C_3N_4/ITO electrode in 0.1 M KCl under visible light. Inset: Photocurrent biased at −0.2 V; (b) Nyquist impedance plots (scatters) for g-C_3N_4 and g-C_3N_4−H^+Cl^- and simulation (lines). The frequency range is from 10^6 to 10^3 Hz, and the perturbation signal is 100 mV. Inset: Dotted area in high magnification and the equivalent circuit mold. The calculated resistances (R_b) before and after protonation were ca. 28 and 1.5 MΩ, respectively.

When exposed to light with an energy greater than its band gap, g-C_3N_4 underwent photodoping and turned from insulator into a photoconductor. The conductivity with negative compared to positive bias voltage was found to be higher, and the onset potential for photocurrent generation was ∼0.1 V. These features are important for future device design.

Another promising field for graphite-like material is battery applications. Due to imperfections and grain effects, the direct conductivity of g-C_3N_4 was however up to now too low for such electrochemical applications. Again, direct use of the protonated material became advantageous. The ionic conductivity of g-C_3N_4−H^+Cl^- was measured by electrochemical impedance spectroscopy using a Pt blocking electrode and was compared with that of the parental material. Figure 3b shows the experimental Nyquist impedance plots for g-C_3N_4−H^+Cl^- and g-C_3N_4 in water. Generally, for an ideal ionic conductor, the spectrum would show a semicircle in the high frequency range for the bulk relaxation of the film and an inclined straight line in the low frequency range representing the conductive contributions. Here, only the spectrum of g-C_3N_4−H^+Cl^- discloses conductance, while that of g-C_3N_4 shows an incomplete very large semicircle, typical for a weak insulator. Using the equivalent circuit mold given in the inset to fit the data, conductivity was found to increase by at least 10 times.

Once polymeric g-C_3N_4 is successfully protonated, further postfunctionalization becomes rather simple. For instance, Cl^- was ion-exchanged by two other functional negative ions, i.e., $Fe(CN)_6^{3-}$ and $PtCl_4^{2-}$. After stirring g-C_3N_4−H^+Cl^- with excess $Fe(CN)_6^{3-}$, a pale blue composite was obtained, which shows a broad UV−vis absorption with a maximum at ca. 700 nm (Figure S3). This is the characteristic charge-transfer absorption of Prussian Blue (PB). Differential pulse voltammetry plots (Figure S4a) of those species show two pairs of typical redox waves, as known for PB.[12] We attribute the formation of PB to the (photo)reduction properties of g-C_3N_4, thus partially converting $Fe(CN)_6^{3-}$ into PB. Similarly, by anion exchange with $PtCl_4^{2-}$ and further reduction by $NaBH_4$, Pt@g-C_3N_4 was obtained. The SEM image (Figure S5a) shows Pt nanopartices (d ∼3.6 nm) uniformly dispersed in the g-C_3N_4 template. We can use this experiment as a measure of homogeneity of the protonation and subsequent ion exchange of the g-C_3N_4, which turns out to be uniform and macroscopically homogeneous. This system is a powerful catalyst, as it was found that PB@g-C_3N_4 and Pt@g-C_3N_4 have electrocatalytic activities toward reduction of H_2O_2 (Figure S4b) and O_2 (Figure S5b), respectively. It is obvious that also electrocatalysis only works with an improved conductivity level of the support, here provided by primary protonation.

In summary, we have described the controllable and reversible protonation of a nanostructures solid, g-C_3N_4. Protonation not only provides better dispersion and a high surface area but also enables the adjustment of electronic band gaps and higher ionic conductivity. The high surface area of protonated g-C_3N_4 could be preserved after recovery by heating and enables improved sintering which allowed for the first time direct measurement of its photoconductivity. Besides, by aid of protonation, other promising g-C_3N_4 based hybrid composites could be facilely prepared by counteranion exchange. Work focused on more detailed photocatalytic and photoelectrochemical studies of functionalized g-C_3N_4 is ongoing.

Acknowledgment. Financial support by the Max Planck Society within framework of project ENERCHEM.

Supporting Information Available: Experimental details, Figure S1−S5. This material is available free of charge via the Internet at http://pubs.acs.org.

References

(1) Kroke, E.; Schwarz, M. *Coord. Chem. Rev.* **2004**, *248*, 493–532.
(2) Liu, A. Y.; Cohen, M. L. *Science* **1989**, *245*, 841–842. Niu, C. M.; Lu, Y. Z.; Lieber, C. M. *Science* **1993**, *261*, 334–337.
(3) Thomas, A.; Fischer, A.; Goettmann, F.; Antonietti, M.; Müller, J.-O.; Schlögl, R.; Carlsson, J. M. *J. Mater. Chem.* **2008**, *18*, 4893–4908.
(4) Zhang, Z.; Leinenweber, K.; Bauer, M.; Garvie, L. A. J.; McMillan, P. F.; Wolf, G. H. *J. Am. Chem. Soc.* **2001**, *123*, 7788–7796. Jurgens, B.; Irran, E.; Senker, J.; Kroll, P.; Muller, H.; Schnick, W. *J. Am. Chem. Soc.* **2003**, *125*, 10288–10300. Kroke, E.; Schwarz, M.; Horath-Bordon, E.; Kroll, P.; Noll, B.; Norman, A. D. *New J. Chem.* **2002**, *26*, 508–512. Horvath-Bordon, E.; Kroke, E.; Svoboda, I.; Fuess, H.; Riedel, R. *New J. Chem.* **2005**, *29*, 693–699. Komatsu, T. *J. Mater. Chem.* **2001**, *11*, 799–801. Gillan, E. G. *Chem. Mater.* **2000**, *12*, 3906–3912. Guo, Q. X.; Xie, Y.; Wang, X. J.; Zhang, S. Y.; Hou, T.; Lv, S. C. *Chem. Commun.* **2004**, 26–27. Lotsch, B. V.; Schnick, W. *Chem.—Eur. J.* **2007**, *13*, 4956–4968. Holst, J. R.; Gillan, E. G. *J. Am. Chem. Soc.* **2008**, *130*, 7373–7379. Bojdys, M. J.; Muller, J. O.; Antonietti, M.; Thomas, A. *Chem.—Eur. J.* **2008**, *14*, 8177–8182. Vinu, A. *Adv. Funct. Mater.* **2008**, *18*, 816–827.
(5) Goettmann, F.; Fischer, A.; Antonietti, M.; Thomas, A. *Angew. Chem., Int. Ed.* **2006**, *45*, 4467–4471.
(6) Fischer, A.; Antonietti, M.; Thomas, A. *Adv. Mater.* **2007**, *19*, 264–267.
(7) Wang, X. C.; Maeda, K.; Thomas, A.; Takanabe, K.; Xin, G.; Carlsson, J. M.; Domen, K.; Antonietti, M. *Nat. Mater.* **2008**, doi:10.1038/nmat2317.
(8) Inoue, S.; Imai, Y.; Uno, K.; Iwakura, Y. *Makromol. Chem.* **1966**, *95*, 236–247.
(9) Ramesh, S.; Ericson, L. M.; Davis, V. A.; Saini, R. K.; Kittrell, C.; Pasquali, M.; Billups, W. E.; Adams, W. W.; Hauge, R. H.; Smalley, R. E. *J.Phys. Chem. B* **2004**, *108*, 8794–8798.
(10) MacDiarmid, A. G. *Angew. Chem., Int. Ed.* **2001**, *40*, 2581–2590.
(11) Huang, J. F.; Luo, H.; Liang, C.; Sun, I. W.; Baker, G. A.; Dai, S. *J. Am. Chem. Soc.* **2005**, *127*, 12784–12785.
(12) Karyakin, A. A. *Electroanal.* **2001**, *13*, 813–819.

JA808329F